Understanding the complex metallic element Mn. II. Geometric frustration in β-Mn, phase stability, and phase transitions

J. Hafner and D. Hobbs

Institut für Materialphysik and Center for Computational Materials Science, Universität Wien, Sensengasse 8/12, A-1090 Wien, Austria

(Received 26 September 2002; revised manuscript received 21 January 2003; published 8 July 2003)

In the preceding paper [D. Hobbs, J. Hafner, and D. Spišák, Phys. Rev. B **68**, 014407 (2003)], we have started an *ab initio* spin-density-functional study of the complex structural and magnetic phase behaviors of Mn by a detailed investigation of α-Mn. It was shown that the complex crystalline and noncollinear antiferromagnetic structures are the results of the conflicting tendencies to maximize simultaneously bond strength and magnetic moment. The present work extends this study to the remaining four polymorphs of Mn. Frustration of antiferromagnetic exchange interaction (which is the driving force leading to noncollinearity in α-Mn) is found to be even stronger in β-Mn. However, in contrast to the current assumption that the magnetic frustration is restricted to the sublattice of the Mn II atoms, with the Mn I atoms remaining nonmagnetic, we find that the antiferromagnetic Mn I-Mn II coupling is strongest, leading to the stabilization of a ferrimagnetic phase upon slight expansion. At equilibrium, a nonmagnetic and a weakly ferrimagnetic phase are energetically virtually degenerate. Antiferromagnetic ground states are found for γ- and δ-Mn (face- and body-centered cubic, respectively), while hexagonal ϵ-Mn is only marginally magnetic at equilibrium. Magnetism strongly influences the mechanical properties of all polymorphs. Due to the stabilization of the antiferromagnetic state on expansion, the γ- and δ-phase are exceptionally soft, whereas β- and ϵ-Mn where magnetism is nearly completely suppressed are mechanically hard. α-Mn is found to be soft in the noncollinear antiferromagnetic state, but hard in the nonmagnetic phase. α-Mn is found to have the lowest energy at ambient pressure, under compression a structural phase transition to ϵ-Mn is predicted, in agreement with recent experiments. In summary, the structural and magnetic phase diagram of even the complex metallic element is well explained by the density-functional theory.

DOI: 10.1103/PhysRevB.68.014408 PACS number(s): 75.25.+z, 61.66.Bi, 75.50.Ee, 61.50.Ah

I. INTRODUCTION

Manganese is known to be the most complex metallic element. At ambient pressure, Mn assumes four different allotropic forms.[1,2] The nonmagnetic α phase stable at room temperature adopts a complex crystal structure with 58 atoms in the cubic elementary cell.[3] Below a Néel temperature of $T_N = 95$ K, α-Mn orders antiferromagnetically in a noncollinear structure.[4,5] The magnetic phase transition is coupled to a tetragonal distortion of the crystal structure.[6] At $T = 1000$ K, a structural phase transition to the β phase occurs. β-Mn is a simple cubic with 20 atoms in the unit cell.[7,8] In the high-temperature state, where β-Mn is stable, it is paramagnetic. The magnetic characterization of quenched specimens has demonstrated[9–11] that although β-Mn remains paramagnetic down to the lowest temperatures, it shows strong spin fluctuations leading also to a large electronic specific heat[12] and to a characteristic temperature dependence of the nuclear spin lattice relaxation rate following a $\sqrt{T}$ behavior.[13] Consequently, β-Mn has been characterized as a spin-liquid. A weak doping with nonmagnetic elements such as Al, In, Sn, or Sb drives a transition to an unconventional spin-glass-like ground state.[11,14]

The face-centered cubic (fcc) γ phase is stable in the narrow temperature interval between 1368 and 1406 K, at higher temperatures up to the melting point of $T_M = 1517$ K the δ-phase has a body-centered cubic (bcc) structure. γ-Mn quenched to room temperature is face-centered tetragonal, the small tetragonal distortion (0.17%) is caused, similar to the distortion of the α phase, by antiferromagnetic ordering.[15] The magnetic ordering transition occurs at a temperature of about $T_N \sim 500$ K.[16,17] γ-Mn may also be stabilized by an epitaxial growth on Cu(100) or Ni(100) substrates.[18,19] The γ-Mn films are tetragonally distorted and assume a high-spin antiferromagnetic ground state of type 1. bcc Mn films have been produced by an epitaxial growth on a Fe(100) substrate.[20] The particular interest in epitaxially stabilized film of γ- and δ-Mn is motivated by the fact that at sufficiently large lattice constants of the substrate, high-moment ferromagnetism has been expected to occur at low temperature.

Recent high-pressure studies[21] found a structural phase transition at $p_c = 158-165$ GPa. A new diffraction peak appearing in the high-pressure phase can be indexed either as the (110) reflection of a bcc lattice, or the (111) reflection of a fcc structure, or as the (101) reflection of a hexagonal close-packed (hcp) structure. The volume changes at the transition are the estimated to be 2.0, 9.4, and 5.6–7.4% for bcc, fcc, and hcp, respectively (assuming an axial ratio between $c/a = 1.55$ and $c/a = 1.65$ for the hcp structure). Because of the smallest volume discontinuity, the bcc structure was adopted as the most likely candidate for the high-pressure ϵ phase of Mn.[21] However, it was pointed out that a bcc structure would be in contradiction to the regular structural trends across the transition metal series, predicting an hcp crystal structure for the group VII elements of the $4d$ and $5d$ series—and also of the $3d$ series if the magnetic moment is quenched by compression. Total energy calculations performed in the local-spin-density approximation (LSDA) also predict the hcp phase of Mn to be lower in energy than either the fcc or bcc phase.[22–25] However, one

should remember that LDA calculations lead to the wrong magnetic ground state for the elements next to Mn in the $3d$ transition series, predicting bcc Cr to be nonmagnetic instead of antiferromagnetic[26] and Fe to be hcp and nonmagnetic instead of bcc and ferromagnetic.[27] For both metals, it has been demonstrated that semilocal corrections to the exchange-correlation functional in the form of a generalized-gradient approximation (GGA) correct the prediction of the magnetic ground state.

Due to the structural complexity of the α and β phases, most attempts to study the electronic and magnetic properties of Mn have been restricted to the simpler γ, δ, and ϵ phases, see Refs. 15, 22–25, 28–39—but this list is not considered to be exhaustive. Although there are some differences in the details, the calculations performed in the LSDA agree on the following.

(i) At equilibrium, the hcp phase is predicted to have the lowest energy, but the structural energy differences are much smaller than those calculated for the other metals of the $3d$ series.[23]

(ii) The calculated equilibrium volume is substantially too low, the error being about twice as large as for the other $3d$-metals (with the exception of iron).

(iii) With increasing atomic volume, all three crystallographic forms of Mn show transitions from a nonmagnetic to a low-spin magnetic phase and further to a high-spin magnetic phase. This holds for both the antiferromagnetic and the ferromagnetic configurations, at the experimental volume antiferromagnetism is generally energetically more favorable than ferromagnetism.[29,30,33,39] However, Fujii *et al.*,[31] Kübler[28], and Moruzzi *et al.*[29] find δ-Mn to be ferromagnetic at equilibrium, the transition to an antiferromagnetic state occurring only in an expanded state. In the intermediate range, ferrimagnetic and spin-spiral structures have been reported.[30,37,38] It also has to be emphasized that all magnetic energy differences are very small around equilibrium.

(iv) Because of the underestimation of the atomic volume, fcc γ-Mn is predicted to be marginally nonmagnetic at equilibrium,[30,39] whereas bcc δ-Mn is found to be weakly ferromagnetic with a moment of about $1\mu_B$. For δ-Mn, this is in conflict with experiment suggesting antiferromagnetic ordering with a similar estimate for the moment,[40] for γ-Mn strong antiferromagnetic ordering with a high experimental moment of $2.3\mu_B$ at room temperature has been reported,[2,41] the Curie temperature of quenched fcc γ-Mn being about 450 K.

(v) Generalized-gradient corrections to the exchange-correlation functional increase the equilibrium volume and stabilize magnetism, leading to improved agreement with experiment.[24,39]

For α- and β-Mn, previous electronic structure calculations[42–44] have been restricted to collinear magnetic calculations, a noncollinear solution was searched using a semiempirical tight-binding technique,[45] but without conclusive results. Only very recently, we have succeeded in performing a full *ab initio* calculation of the crystalline and the noncollinear magnetic structures of α-Mn[46,47] (hereafter, this work will be referred to as I). We have demonstrated that the outstanding structural and magnetic properties of Mn arise from conflicting tendencies related to the half-filled d band: (i) According to Hund's rule, the magnetic spin-moment should be maximum; (ii) for a half-filled band only bonding and no antibonding states are expected to be occupied, strong bonding leading to short interatomic distances. However, close interatomic distances tend to quench magnetism. The complex crystal structure of α-Mn is the result of a compromise between these two conflicting tendencies: α-Mn may be considered as an intermetallic compound formed by large, strongly magnetic (Mn I, Mn II) and small, weakly magnetic (Mn III) or even nearly unmagnetic (Mn IV) atoms. In fact the structure of α-Mn is isotypic to that of χ-phase Fe-Cr-Mo alloys. The noncollinear magnetic structure of α-Mn is due to the fact that the small Mn IV atoms arranged on triangular faces of the coordination polyhedra around the large Mn I atoms are not entirely unmagnetic. Their frustrated antiferromagnetic coupling leads to a local spin arrangement similar to that in the Néel phase of a frustrated triangular antiferromagnet. The noncollinear orientation of the magnetic moments on the other Mn atoms is a direct consequence of this basic frustration.

Frustration is also believed to be of central importance for understanding the strong spin-fluctuations characteristic for quenched β-Mn.[11,48] In fully frustrated lattices such as the Kagomé or the pyrochlore lattices, the frustration of antiferromagnetic interactions in local triangular rings overcomes any magnetic ordering and these systems behave as classical or quantum spin liquids.[49–52] The purely geometrical picture of frustration applying to these structures, however, cannot be transferred to β-Mn without modifications. The $A13$ structure of β-Mn (space group $P4_132$)[7,8,53] contains 20 Mn atoms on two inequivalent sites, Mn I ($8c$ sites) and Mn II ($12d$ sites). Figure 1(a) shows a perspective view of the unit cell of β-Mn. The structure is rather difficult to describe and for the full lattice, the character of the geometrical frustration is not evident. The magnetic characterization of β-Mn, however, has led to the assumption that the magnetic properties can be interpreted by considering paramagnetic moments on the Mn II sites only, the Mn I atoms being almost nonmagnetic.[11,51] The Mn II sublattice shown in Fig. 1(b) can be regarded as a network of corner-sharing triangles—in this respect, the sublattice is similar to the two-dimensional Kagomé lattice. In β-Mn, however, the triangular network is not planar. Each triangle is perpendicular to one of the [111] axes such that neighboring triangles form an angle ϕ satisfying $\cos\phi = 1/3$. Hence, the Mn II-sublattice has been termed as ''three-dimensional Kagomé lattice.'' Canals and Lacroix[48] have shown that for a classical Heisenberg Hamiltonian with antiferromagnetic nearest-neighbor interactions on the Mn II-sublattice only, the ground state is a degenerate spin spiral with a wave vector $[qqq]$ along the body diagonal. It is of evident interest to verify these conjectures by a spin-polarized calculation of the electronic structure.

According to the augmented spherical wave (ASW) calculations of Sliwko *et al.*,[42] β-Mn is nonmagnetic in the experimentally determined structure. At expanded volume ($\triangle a = +3\%$), β Mn is reported to be ferrimagnetic with small moments on both sites: $\mu(\text{Mn I}) = 0.15\mu_B$ and $\mu(\text{Mn II}) = -0.57\mu_B$. Hence, the assumption of entirely

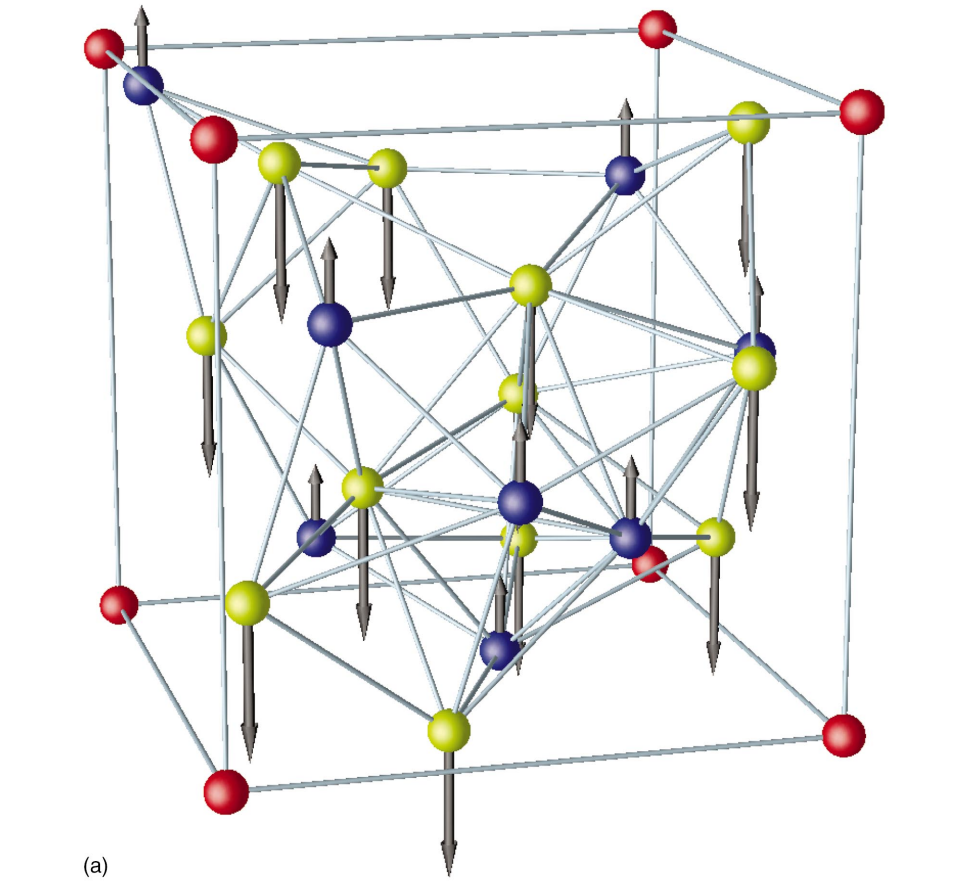

(a)

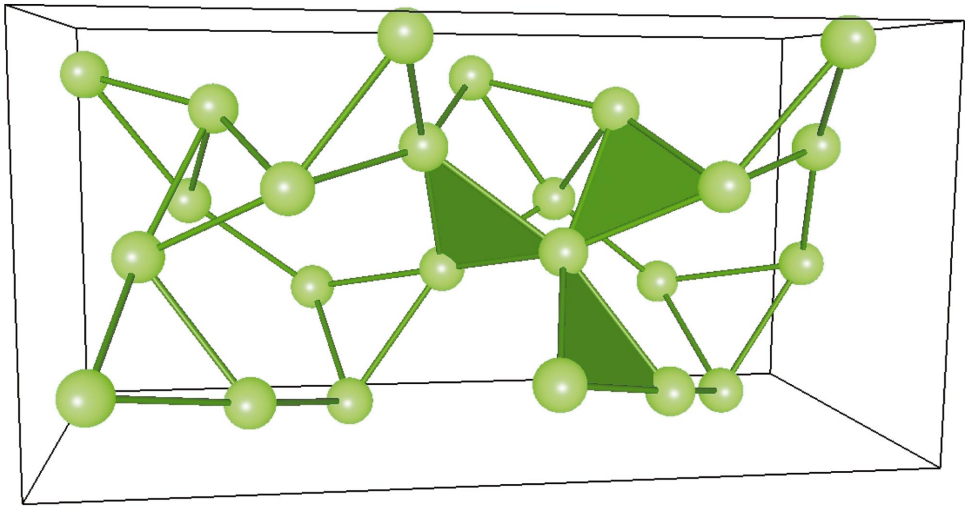

(b)

FIG. 1. (Color) (a) Pictorial representation of the unit cell of β-Mn. Blue balls represent Mn I atoms, light green balls Mn II atoms (red balls merely mark the corners of the unit cell). The shortest nearest-neighbor bonds are drawn. The arrows visualize the ferrimagnetic moments calculated at a slightly expanded volume. The smaller Mn I moments are oriented along the positive z direction, the larger Mn II moments are oriented antiparallel to the Mn I moments. (b) Mn II sublattice in a doubled unit cell of β-Mn, consisting of a network of corner-sharing triangles. All triangle planes are normal to one of the [111] axes. One of the "distorted wind mill" elements formed by three nearly regular corner-sharing triangles is highlighted by the shading of the triangles. The angle ϕ between two triangles satisfies $\cos\phi = 1/3$; Cf. text.

nonmagnetic Mn I atoms is not confirmed. Asada[44] has used the linearized muffin-tin-orbital (LMTO) technique to calculate the electronic and magnetic structures of β-Mn. At the equilibrium lattice constant, a ferrimagnetic phase with moments of $\mu(\text{Mn I}) = 0.2\ \mu_B$ and $\mu(\text{Mn II}) = -1.25\mu_B$ was found to be more stable than the nonmagnetic state. In addition, Asada considered a "nearly least frustrated antiferromagnetic" (NLF-AF) phase in which the moments on all Mn I sites are all parallel, whereas the Mn II moments are forced to point into different directions such as to release as far as possible the frustration on the triangular Mn II sublattice (but no indication how this is achieved is given in the paper). For this NLF-AF structure, Asada reports for the experimental density almost vanishing Mn I moments and $|\mu(\text{Mn II})| = 2.0\ \mu_B$, and for the equilibrium atomic volume (which is found to be 3 pct larger than in experiment), $\mu(\text{Mn I}) = 0.2\ \mu_B$ and $|\mu(\text{Mn II})| = 2.38\mu_B$.

In the present work, we extend our study of the structural and magnetic properties of Mn, started in *I* with the investigation of α-Mn, to the remaining four polymorphs. As in *I*,

TABLE I. Crystallographic information on β-Mn.

Space group:	$P4_132$	$a=6.29$ Å (expt.), $a=6.007$ Å (theor)
Atom	Wyckoff position	Coordinates
Mn I	$8c$	(x,x,x), $(1/2+x, 1/2-x, -x)$, $(1/2-x, -x, -x\ 1/2+x)$, $(-x,1/2+x,1/2-x)$, $(3/4-x,3/4-x,3/4-x)$, $(1/4-x,3/4+x,1/4+x)$, $(1/4+x,1/4-x,3/4+x)$, $(3/4+x,1/4+x,1/4-x)$ $x(\text{expt.})=0.0061$,[a] 0.0636[b] $x(\text{theor.})=0.059$,[c] 0.060[d]
Mn II	$12d$	$(1/8,y,1/4+y)$, $(y,1/4+y,1/8)$, $(1/4+y,1/8,y)$, $(3/8,-y,3/4+y)$, $(-y,3/4+y,3/8)$, $(3/4+y,3/8,-y)$, $(5/8,1/2-y,3/4-y)$, $(1/2-y,3/4-y,5/8)$, $(3/4-y,5/8,1/2-y)$, $(7/8,1/2+y,1/4-y)$, $(1/2+y,1/4-y,7/8)$, $(1/4-y,7/8,1/2+y)$, $y(\text{expt.})=0.206$,[a] 0.2022[b] $y(\text{theor})=0.190$,[c] 0.200[d]

[a]Reference 7.
[b]Reference 53.
[c]At the theoretical equilibrium lattice constant.
[d]At the experimental lattice constant.

we perform first-principles spin-density functional calculations of the crystalline, electronic, and magnetic structures using the projector-augmented wave technique.[54,55] The exchange-correlation functional[56] proposed by Perdew and Zunger,[57] together with the spin interpolation of von Barth and Hedin[55] and the generalized-gradient corrections[58] of Perdew *et al.*,[59] has been used. For any further technical aspects, we refer to *I*. The paper is organized as follows. In Sec. II, we discuss the properties of β-Mn, with particular attention to the magnetic structure and to the frustration of the magnetic interactions. Section III presents the results for the high-symmetry polymorphs γ-, δ-, and ϵ-Mn. Section IV summarizes the structural energy of all allotropes and discusses the possibility of a pressure-induced phase transition. We conclude in Sec. V.

II. CRYSTALLINE AND MAGNETIC STRUCTURES OF β-Mn

A. Crystal structure and magnetic frustration

The crystallographic information on β-Mn ($A13$-type) is summarized in Table I, a picture of the unit cell is given in Fig. 1(a). The structure is simple cubic, space group $P4_132$ (or $P4_332$) with $a=6.29$ Å, see Refs. 7,8,53. There are two inequivalent Mn sites: Mn I in ($8c$) position and Mn II in ($12d$) position. It is important to emphasize that—as already noted for the $A12$ structure of α-Mn—most examples of the $A13$ structure occur as binary alloys, e.g., Fe_2Re_3. The structure is more compact around the Mn I sites. Each Mn I atom is surrounded by a distorted icosahedron whose vertices are occupied by three Mn I at a distance $d_1(\text{Mn I-Mn I})=0.376a$ (where a is the cubic lattice constant) and nine Mn II at distances of $d(\text{Mn I-Mn II})=0.4011a$, $0.4253a$, and $0.4256a$. The coordination polyhedron around Mn II is a Frank-Kasper polyhedron with coordination number (CN) 14 occupied by six Mn I atoms at the distances listed above and eight Mn II, three at $d_1(\text{Mn II-Mn II})=0.4139a$ and $d_2(\text{Mn II-Mn II})=0.4225a$ each and two at $d_3(\text{Mn II-Mn II})=0.5153a$ (all distances are calculated using the internal parameters of Preston[7]). Hence, the local coordination is similar to that of the Mn IV and Mn III sites in α-Mn surrounded by an icosahedron and a CN13 Frank-Kasper polyhedron, respectively. All these polyhedra may be decomposed into more or less distorted tetrahedra.

Due to the low site-symmetry [trigonal around the [111] axis and orthorhombic with the symmetry axis (110)], the β-Mn structure is difficult to describe. O'Keefe and Anderson[8] have shown that a certain class of structures including β-Mn may be described in terms of a dense packing of identical infinite cylinders (''rod packing''). In the real structures, these rods are replaced by strings of atoms or of group of atoms. In the case of β-Mn, the rods consist of a repeating sequence of four Mn I-Mn II_3 tetrahedra and Mn II_6 ''metaprisms'' centered by Mn I [a metaprism is a polyhedron intermediate between an octahedron ($\hat{=}$ triangular antiprism, parallel triangles rotated by 60° with respect to each other) and a triangular prism (rotation angle zero), in the β-Mn metaprism the rotation angle is $\cos^{-1}(11/14)=38.2°$ in the ideal geometry]. An ideal value for the free parameter y of the Mn II sites is defined by the requirement that the equilateral faces of the metaprisms be congruent (and hence as many of the shortest Mn II-Mn II distances as possible are equal), leading to $y=0.2035$. The parameter x in the coordinates of the Mn I sites is determined by the condition that the six shortest Mn I-Mn II distances be all equal—this happens for $x=0.0678$. The measured structural parameters are very close to these ideal values. With these parameters, the ratio of the shortest Mn I-Mn II distance to Mn II-Mn II distance is 1.055 so that the Mn I-Mn II_3 tetrahedra are nearly regular (the ratio is 1.061 in the real structure).

The connection with the network of corner-sharing triangles forming the Mn II sublattice [see also Fig. 1(b)] and used for the discussion of the geometric frustration of the magnetic interactions[11,48] may be established by noting that neighboring ''rods'' share Mn II atoms such that $Mn\,II_6$ metaprisms share corners. However, in view of the closeness of the shortest Mn I-Mn II and Mn II-Mn II distances, the crystal geometry provides little justification for a discussion of frustration in terms of the magnetic coupling between the Mn II atoms alone.

In view of the importance of the nearly regular Mn I-$Mn\,II_3$ tetrahedra in the structure, the proper reference for discussing frustration may be rather the tetrahedral network of the majority atoms in a Laves phase—indeed YMn_2 and RMn_2 compounds (R=rare earth metal) have been extensively examined for frustration effects.[60–62] The coordination of the majority atoms in the Laves phases is icosahedral, the coordination polyhedron of the larger minority atoms is a CN16 Friauf-Frank-Kasper polyhedron whose vertices are occupied by 12 majority and 4 minority atoms. Hence, a unifying feature of the β-Mn and Laves structures is that both are polytetrahedral. In the Mn-based Laves phases, the ground state is magnetically disordered due to frustration, strong antiferromagnetic correlations between the Mn atoms are suppressed. The similarity between the β-Mn and the Laves phases is further supported by the fact that nonmagnetic impurities substituting for Mn induce a spin-liquid to spin-glass transition in both cases.[11]

The assumption that only the Mn II atoms carry a paramagnetic moment, while the Mn I atoms are nonmagnetic is based on the interpretation of the nuclear-magnetic-resonance (NMR) spectra[11,13,14,63] and of the magnetic neutron-scattering data.[11] Due to the low site symmetry, both Mn sites in β-Mn possess an electric-field gradient, which on site I has axial symmetry and on site II is nonaxial. The difference in symmetry allows a unique assignment of the NMR signals. Nuclear quadrupole resonance (NQR) measurements lead to a nuclear quadrupole coupling constant of $\sim$30 MHz at site II and a significantly smaller one of only 1.5–7 MHz at site I (Refs. 11,13,63). The presence of a zero-field NQR signal is a clear indication of the absence of magnetic ordering. Upon a modest degree of doping with Al, the NQR signals disappear rapidly. Instead, zero-field resonances in the NMR spectra appear at low and high frequencies, around 10–20 MHz and 80–100 MHz at an Al concentration of 10–20%. Assuming a hyperfine coupling constant of -80–-100 Oe/μ_B (which is the same as in α-Mn, see Ref. 4), this leads to static moments of $0.1\mu_B$–$0.2\mu_B$ and $\sim 1\mu_B$, assigned to sites I and II, respectively.[11,13] The different magnetic character of both types of sites appears also in the nuclear spin-lattice relaxation rate $1/T_1$, which is about 20 times larger at site II than at site I. Neutron-scattering studies reveal strong antiferromagnetic spin fluctuations in pure β-Mn, which persist even in the spin-glass-like state of β-$Mn_{1-x}Al_x$ ($x>0.03$), integration of the quasielastic neutron spectra over the entire Brillouin zone leads to Mn II moments in agreement with those from the NMR spectra. This has led to the assumption that the paramagnetic moments in the spin-liquid phase of pure β-Mn are of the same order of magnitude as the static disordered moments in the spin-glass-like β-$Mn_{1-x}Al$ alloys.

Little attention has been paid so far to the implication of the assumption of nonmagnetic Mn I atoms on the electronic structure. Nakamura *et al.*[11] only note . . . ''this suggests that the $3d$ electron levels of site-I atoms are far below the Fermi level and/or the site I contribution to the Fermi-level density of states is small.'' In view of the crystal structure, such a drastic difference in local densities of states of Mn I and Mn II atoms would be highly surprising.

B. Crystalline and magnetic structures—Theory

We have performed a simultaneous optimization of the crystalline, electronic, and magnetic structures of β-Mn without any symmetry constraint and allowing for nonmagnetic, collinear, and noncollinear magnetic configurations. Magnetization has been described using the unconstrained vector-field approach reviewed in detail in *I*. Due to the absence of symmetry constraints, all Mn atoms within the unit cell are considered as inequivalent and, in principle, the calculations admit for different moments on each site—this is important in view of the geometric frustration of the magnetic interactions. In this respect our calculations are similar to the setup used by Asada[44] in his NLF-AF structure. Brillouin-zone integrations have been performed on a $4\times4\times4$ grid (extending over the entire Brillouin zone in the absence of symmetry constraints) and using a modest smearing of the one-electron levels to improve convergence (see *I* for further details).

Our results for the total energy, internal structural parameters, and magnetic moments are summarized in Fig. 2. The calculated equilibrium atomic volume is $V=10.84$ Å^3 ($a=6.007$ Å), corresponding to an underestimate of -13.5 pct. in the volume (-4.7 pct. in the lattice constant) compared to the experimental value of Preston.[7] However, one has to bear in mind that the experimental value refers to a high-temperature phase quenched to room temperature. Still, the equilibrium volume is probably somewhat underestimated—like for all $3d$ antiferromagnets (Cr, α-, and β-Mn, and γ-Fe—cf. also the discussion in *I*). The internal structural parameters are found to be almost independent of the atomic volume; at equilibrium, we calculate $x=0.059$ and $y=0.195$; at the experimental volume, we find $x=0.060$ and $y=0.20$ in very good agreement with the experimental values (see also Table I).

At all atomic volumes lower than about 11.8 Å^3, nonmagnetic and an almost ferrimagnetic β-Mn (with a small magnetic moment of $\sim 0.25\mu_B$ at sites II and essentially nonmagnetic Mn I atoms) are energetically degenerate within the accuracy of our calculations which is estimated to be a few meV/atom. At expanded volumes, a ferrimagnetic state with large moments at sites II and smaller, but by no means negligible, moments at sites I develops (see Figs. 1 and 2) in agreement with the results of Sliwko *et al.*[42] and of Asada.[44] At the experimental volume ($V=12.44$ Å^3), Sliwko *et al.* find β-Mn to be nonmagnetic, while Asada calculates moments of $\sim 0.2\mu_B$ and $\sim 1.25\mu_B$ for sites Mn I and Mn II, respectively, in a constrained ferrimagnetic configuration and

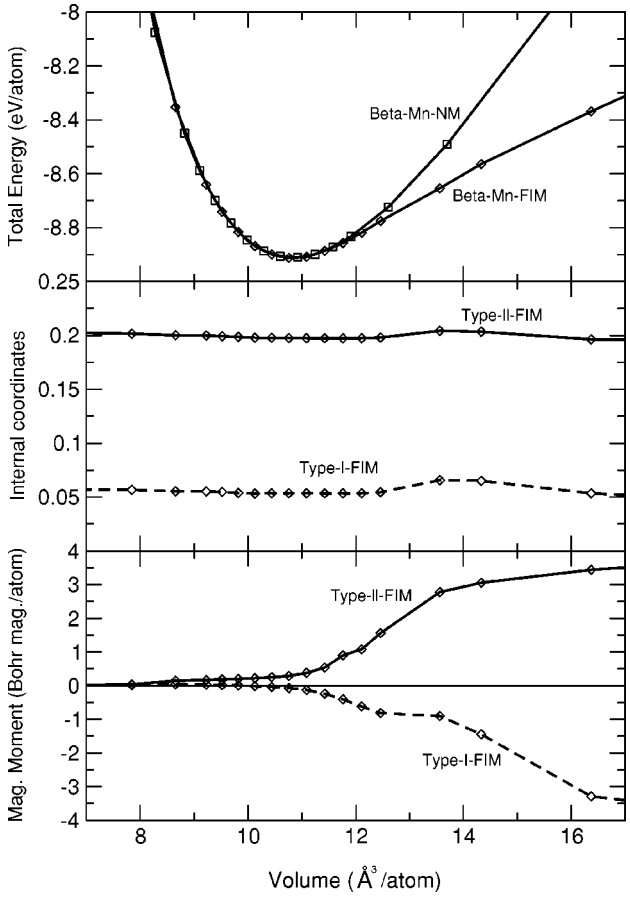

FIG. 2. Total energy, internal structural parameters (x for sites I, $1/2+y$ for sites II, cf. Table I), and local ferrimagnetic moments for β-Mn.

even larger Mn II moments in a noncollinear, but not further characterized ''nearly least frustrated antiferromagnetic'' structure. We have also made several attempts to find a possible noncollinear spin configuration, but independent of the initialization of the magnetic structure, the calculations always relaxed to a nonmagnetic or to a nearly collinear ferrimagnetic state, depending on volume.

The volume dependence of the local magnetic moments shows a very unusual behavior: at a strongly expanded volume, both the Mn I and the Mn II moments are as large as $3-4\mu_B$. The limiting value of $5\mu_B$ set by Hund's rule would, however, be approached only at much larger volumes where a fully occupied $4s$ band begins to separate from the $3d$ band (cf. the investigation of the large-volume magnetic behavior of the $3d$ metals by Moruzzi and Marcus[30]). At smaller volumes, the magnetic moment of the Mn I atoms is reduced more rapidly, but on both sites the transition to a nonmagnetic state is extremely sluggish, a small moment persists over a very large volume range. This is a strange behavior—for all $3d$ metals in one of the common metallic structures (including bcc and fcc Mn), it has been shown[29,30] that the volume dependence of the magnetic moment is necessarily singular, the magnetic to nonmagnetic transition being usually of second order—for the more complex behavior of γ- and δ-Mn, see also the following section. We have verified that the persistence of a small magnetization at an increased density is not the result of an insufficient convergence of our calculations. To understand this behavior, we must remember that the calculations are performed with the version of the PAW for noncollinear magnetizations in an unconstrained vector-field description. These calculations (like those for α-Mn reported in *I*) are performed without any symmetry constraint—hence this setup admits for magnetic fluctuations within the unit cell coupled to local distortions from the perfect structure. In the multidimensional parameter space of the crystalline and magnetic coordinates, the magnetic potential-energy surface is extremely flat. In practice, the fluctuations in the magnetization from one Mn I or Mn II atom to another are very small in magnitude and direction, and the graphs report the average moments. Imposing symmetry constraints on the atomic positions and collinearity of the magnetic moments does not lead to a qualitative change of this picture: the ferrimagnetic minimum disappears already at $V\sim 10$ Å^3, but the curvature of the moment vs volume relation remains the same. Our result of degenerate nonmagnetic and weakly ferrimagnetic states at equilibrium is—within the limits of a mean-field description—not inconsistent with the experimental characterization of β-Mn as a spin liquid.

This persistence of the magnetic moment over a wide range of densities in β-Mn is indicative of a high degree of frustration of the magnetic interactions—a similar behavior has been found for the Mn IV sites in α-Mn if the directions of the magnetic moments are constrained to a collinear orientation (see Fig. 2 in *I*). In α-Mn, the antiferromagnetic interaction between the Mn IV atoms is highly frustrated, as these atoms occupy triangular facets on the CN16 polyhedron around Mn I. If the collinear constraint is relaxed, a local spin arrangement similar to the Néel state of a triangular antiferromagnet is assumed and the Mn IV moments show the expected critical behavior at the onset of noncollinear magnetic ordering (which is triggered precisely by the formation of static moments on the Mn IV sites). In contrast to α-Mn, the β-Mn lattice is fully frustrated and the frustration cannot be eliminated by a noncollinear spin arrangement.

The ferrimagnetic ordering of expanded β-Mn with a ferromagnetic order on both type-I and type-II sublattices is a rather surprising result, which contradicts the assumption underlying the interpretation of the observed magnetic character of β-Mn, namely, the antiferromagnetic coupling between the Mn II atoms is much stronger than the Mn I–Mn II interaction. To the contrary, the ferrimagnetic order shows that the dominant antiferromagnetic interaction is that between inequivalent atoms. A ferrimagnetic ground state of an element is by itself a rather surprising result, although it is rather common in intermetallic compounds. The possibility of ferrimagnetic ordering in bcc δ-Mn has been discussed by Moruzzi and Marcus[30] and by Sliwko *et al.*[37] They reported a ferromagnetic ground state at equilibrium, ferrimagnetic CsCl-type ordering at an expansion of about 3 pct., and a transition to type-1 (CsCl-type) antiferromagnetism at 8 pct. expansion. Hence, ferrimagnetism appears as a possible intermediate state between ferromagnetic and antiferromag-

TABLE II. Equilibrium atomic volume V, magnetic ground state (AFM—antiferromagnetic, type 1 or 2, FIM—ferrimagnetic, NCL—noncollinear), structural enthalpy difference ΔH at zero pressure relative to the α phase, bulk modulus B_0, and its pressure-derivative B_0' of all five Mn polymorphs. Cf. text.

Phase	Magnetic State	V (theor) (Å^3)	V (exp) (Å^3)	ΔH (meV)	B_0 (theor) (GPa)	B_0 (exp) (GPa)	B_0'(theor)	B_0'(exp)
α-Mn	AFM-NCL	11.08	12.05[a]	0	188	158[b]	6.0	4.6[b]
β-Mn	FIM	10.84	12.44[c]	63	269		4.7	
γ-Mn	AFM1	11.16	12.95[d]	67	144		7.4	
δ-Mn	AFM2	11.12		146	166		6.8	
ϵ-Mn	AFM	10.72		61	246		5.2	

[a]Reference 6.
[b]Reference 21.
[c]Reference 7, room-temperature measurements on quenched specimens.
[d]Reference 68, value obtained by extrapolation of high-temperature data to room temperature.

netic orderings. Due to the inequivalence of the two types of Mn-sites, ferrimagnetism in β-Mn appears to be even more likely. However, Mohn *et al.*[38] have argued that the ferrimagnetism in δ-Mn corresponds only to a collinear projection of an energetically more favorable spin-spiral state. Similarly, we cannot entirely discard the possibility that the ferrimagnetic state of an expanded β-Mn represents only a local minimum. The change in the magnetic character of β-Mn by alloying with nonmagnetic elements such as Al is due to two effects: (i) expansion of the crystal lattice leading to a stabilization of the local moments and (ii) randomness of the magnetic interactions. It remains to be seen whether this randomness is necessary to stabilize the spin-glass-like ground state or whether this is also the ground-state of the expanded β-Mn.

However, even for δ-Mn, our new results demonstrate that type-2 antiferromagnetism is energetically more favorable than either ferromagnetism, ferrimagnetism, or type-1 antiferromagnetism, see also the following section. In the study of Moruzzi and Marcus,[30] other types of antiferromagnetism have not been considered, because they have mixtures of parallel and antiparallel nearest-neighbor moments and this was expected to lead to an increased magnetic energy.

C. Bulk modulus

The bulk modulus of β-Mn has been calculated by fitting the energy vs volume data to a Birch-Murnaghan equation[65] and to the ''universal equation of state'' proposed by Vinet *et al.*[66] Both fits agree on a very high value of the bulk modulus of $B_0 = 269 \pm 2$ GPa and a pressure derivative $B_0' = \partial B_0 / \partial p = 4.7$ for a ferrimagnetic β-Mn at equilibrium (see also Table II), for nonmagnetic β-Mn an even higher value of $B_0 \sim 300$ GPa results. This is a rather remarkable result. Whereas in *I*, we had calculated for α-Mn a bulk modulus of $B_0 = 188$ GPa which is softer than that of the other ferromagnetic or antiferromagnetic metals, we now find β-Mn to be much harder, with a bulk modulus comparable to that of the nonmagnetic $4d$ and $5d$ metals.

D. Electronic structure of β-Mn

Figure 3 presents our results for the total, site-, spin-, and angular-momentum-decomposed electronic density of states of β-Mn at two different densities. At the equilibrium density where the nonmagnetic and weakly ferrimagnetic states of β-Mn are energetically degenerate, only in the ferrimagnetic state very weak exchange splitting in the local density of state (DOS) at the Mn II sites of $\sim$0.2 eV is recognizable. At this density, the local DOS of β-Mn is very similar to the local DOS at the Mn III and Mn IV sites in α-Mn (cf. Fig. 7 in *I*)—this is not unexpected as the local environments are very similar as well: icosahedral and CN14 coordination at sites I and II in β-Mn, icosahedral and CN13 at sites IV and III in α-Mn. The total DOS at the Fermi level is rather low ($\sim$ 0.8 states/eV atom spin)—this is about one order of magnitude lower than deduced from the specific-heat measurements,[11] confirming the strong enhancement due to spin fluctuations. The local DOS's shown here are also in good agreement with those reported by Sliwko *et al.*[42] At an expanded volume, the large ferrimagnetic moments are reflected in a rather large exchange splitting. However, we note also rather pronounced differences in the majority and minority DOS's, indicating a substantial variation of the exchange splitting through the Brillouin zone. At both densities, the local DOS's at sites I and II are quite similar—band width and center of gravity of the d bands are almost the same. This is expected from the local geometries, but in marked contradiction to the speculations put forward to justify the assumption of a vanishing magnetic coupling between Mn I and Mn II atoms. Altogether the LSD calculations suggest that a fundamental modification of the interpretation of the magnetic behavior of β-Mn, based on geometric frustration on the type-II sublattice alone, will be necessary.

III. STRUCTURAL AND MAGNETIC ENERGIES OF THE HIGHLY SYMMETRIC POLYMORPHS

As recapitulated in the Introduction, the magnetic properties of the highly symmetric polymorphs of Mn have been discussed repeatedly in the literature. However, most of these studies are concerned with just one structural and magnetic configuration, and with the exception of the work of Asada and Terakura[24] and of Eder *et al.*[39] gradient corrections to the exchange-correlation functional (now known to be essential for a correct prediction of the cohesive and magnetic prop-

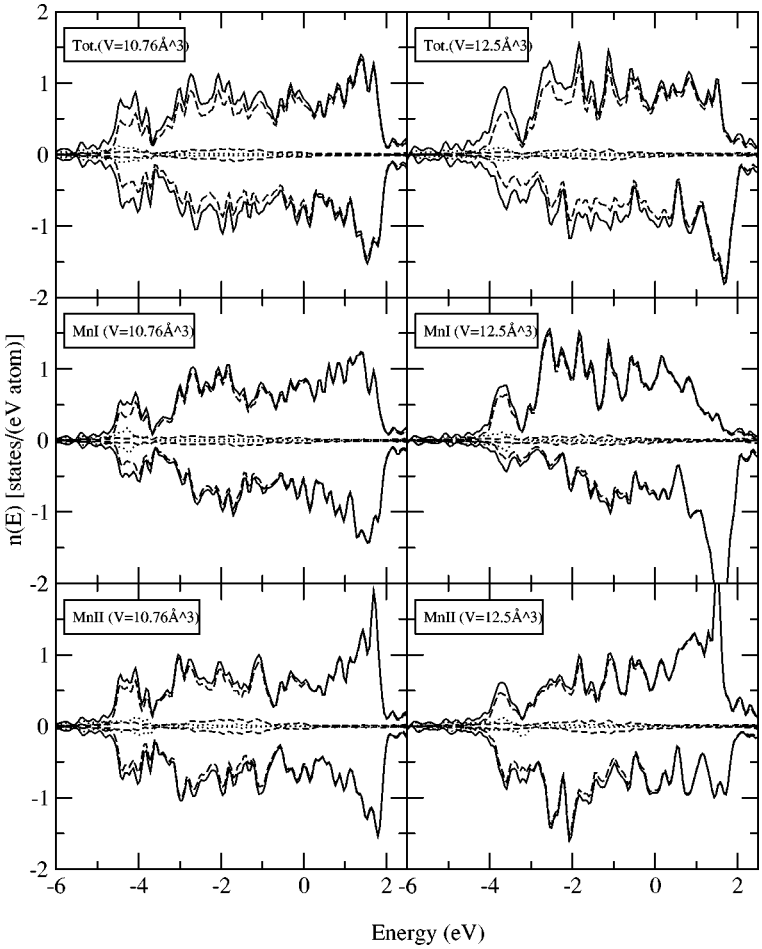

FIG. 3. Total, site- and angular-momentum decomposed spin-polarized electronic density of states of the weakly ferrimagnetic phase β-Mn. The left panels show the DOS calculated at the theoretical equilibrium density, the right panels the DOS at the experimental density. Note that at equilibrium the nonmagnetic and ferrimagnetic phases are energetically degenerate. Full line—total DOS, dotted—short, and long-dashed lines represent the *s*, *p*, and *d* components, respectively. The energy zero is at the Fermi level.

erties of the $3d$-metals) have been neglected. Also so far no attempt has been made to determine the structural energy-difference between α- and β-Mn and the more compact high-temperature polymorphs. Therefore γ-, δ-, and ϵ-Mn have been included in our study. Our results for the total energies and magnetic moments as a function of volume are summarized in Fig. 4.

A. Face-centered cubic γ-Mn

We have compared the paramagnetic, ferromagnetic, type-1, and type-2 antiferromagnetic configurations of γ-Mn. The type-1 (CuAu-type) solution is lowest in energy from the onset of magnetic ordering at $V \sim 10$ Å^3 up to the free-atom limit. Type-2 antiferromagnetism (the sign of the

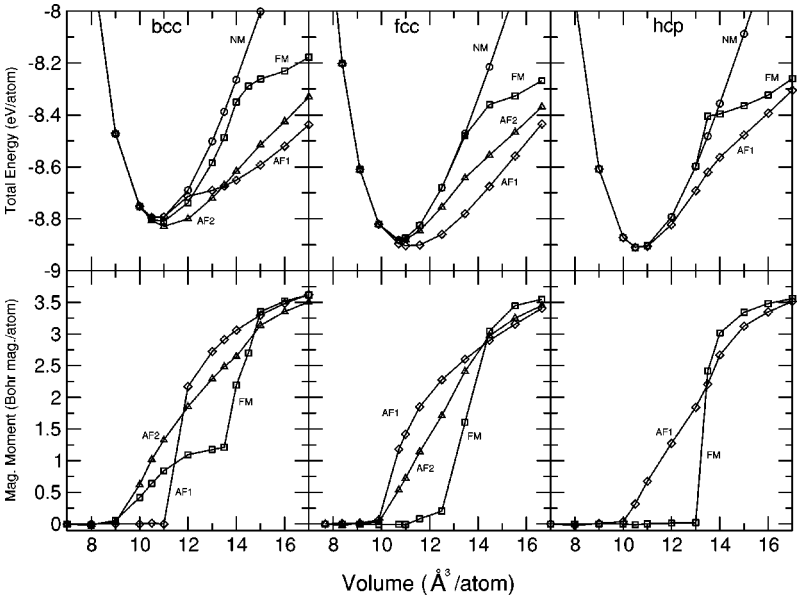

FIG. 4. Total energy and magnetic moment in paramagnetic, ferromagnetic, and antiferromagnetic fcc γ-Mn, bcc δ-Mn, and hcp ϵ-Mn vs volume. Circles, squares, and triangles represent the calculated values, the continuous lines are merely a guide to the eye.

moment alternates between planes stacked along [111]) is also energetically more favorable than ferromagnetism—a ferromagnetic solution exists only for atomic volumes larger than about 12.5 Å^3. At the equilibrium volume of $V = 11.1$ Å^3, the antiferromagnetic moment is $1.6\mu_B$. Both the volume and the magnetic moment are somewhat underestimated compared to the values estimated for quenched γ-Mn ($V = 12.4$ Å^3, $\mu \simeq 2.4\mu_B$), the moment calculated at the experimental volume ($\mu \simeq 2.3\mu_B$) agrees well with experiment. Compared to the LSD calculations of Moruzzi *et al.*[33] and Eder,[39] the onset of magnetic ordering is shifted to higher densities and the equilibrium volume is increased, improving agreement with experiment. This agrees with the well-known tendency of the GGA to reduce the bond strength, to stabilize magnetic ordering, and to produce substantially larger magnetovolume effects than the purely local LSDA.[27] However, the present all-electron PAW calculations predict a smaller effect of the GGA on the equilibrium volume and a smaller magnetovolume effect than the calculations of Eder *et al.*[39] using ultrasoft pseudopotentials, although both sets of calculations produce almost identical results for the magnetic moment as a function of volume and for the electronic DOS at a fixed volume. The difference between the all-electron and pseudopotential calculations can be traced back to an isotropic contribution of the gradient terms to the internal pressure arising mostly from the region where valence- and core electrons and spin densities overlap. In this region, the difference between the all-electron and pseudodensities becomes important—the effect is larger for the magnetic terms because the spin densities tend to be more localized. This difference cannot be eliminated by nonlinear core corrections, it can be made to disappear only by choosing a very hard pseudopotential requiring also a very extended basis set. We also note that the difference between the all-electron and the pseudopotential calculations is larger in Mn than in all other magnetic $3d$ metals.

For an antiferromagnetic γ-Mn, we calculate a very low bulk modulus of $B_0 = 144$ GPa which is one half the value found for β-Mn and also smaller as the bulk modulus of α-Mn, cf. Table II. However, the bulkmodulus increases rapidly under compression, $B_0' = 7.4$. Asada[24] reports even smaller values of $B_0 = 107$ GPa and 86 GPa in his GGA calculations using an LMTO method and the atomic sphere approximation (ASA) producing a somewhat larger equilibrium volume. The tendency of the LMTO-ASA to produce larger equilibrium volume than full-potential calculations is well known, but the origin of the difference between the data reported in the two publications cited under Ref. 24 remains unclear. Moruzzi *et al.*[33] also calculate a very low bulk modulus of $B_0 = 110$ GPa using the ASW method.

We have not considered the magnetically induced tetragonal distortion[41] of γ-Mn. The energy lowering induced by this distortion was c alculated to be about 13 meV/atom by the LMTO-ASA method.[15] There have also been suggestions that this lattice distortion is coupled to a noncollinear ordering in the form of a multiple spin-density wave,[16,67] but the experimental evidence refers rather to Mn-based alloys than to pure γ-Mn.

B. Body-centered cubic δ-Mn

For a bcc δ-Mn, our calculations predict a transition from type-2 (in-plane) to type-1 (CsCl-type) antiferromagnetic ordering on expansion. Type-2 ordering sets in at a substantially higher density ($V \sim 9$ Å^3) than type-1 ordering (onset at $V \sim 11$ Å^3). The onset of low-moment ferromagnetic ordering is found at about the same density as type-1 antiferromagnetism. Up to a volume of ~ 12.2 Å^3, ferromagnetism is energetically more favorable than type-1 antiferromagnetism. At a critical volume of ~ 13.5 Å^3, a low-spin/high-spin transition in the ferromagnetic phase is observed.

Our results are qualitatively similar to the LSDA results of Kübler and of Moruzzi *et al.*,[28–30] but the onset of magnetic ordering is shifted to higher densities as already mentioned for γ-Mn. It is interesting to note that type-2 antiferromagnetism (this type of ordering was not considered in previous calculations) is found to be preferred over type-1 antiferromagnetism. The essential difference is that in the type-1 structure, all nearest neighbors have antiparallel moments, whereas in the type-2 structure both parallel and antiparallel orientations are found. This feature, the fact that at equilibrium the ferromagnetism is energetically intermediate between both antiferromagnetic variants, and the existence of a low- to high-spin transition shows that in δ-Mn, there is a competition between ferromagnetic and antiferromagnetic exchange interactions varying strongly with the interatomic distance. In the work of Moruzzi and Marcus[30] and of Sliwko *et al.*,[37] a ferrimagnetic phase was found to have the lowest energy in the transition region. Mohn *et al.*[38] have argued that the ferrimagnetic structure is just a projection of a spin-spiral state onto a collinear spin-quantization axis. Using a version of the ASW method admitting spin-spiral structures and the generalized Bloch-theorem of Herring,[64] the dispersion relations of spin-spiral states were explored. Depending on the atomic volume up to seven, (meta) stable spin-spiral states were found. In the transition region between the ferromagnetic and the type-1 antiferromagnetic phases, these spin-spiral states can be about 10–25 meV/atom lower in energy than either collinear state. Here, we have not considered spin-spiral states, but the magnetic energy difference favoring type-2 antiferromagnetism is definitely larger than the stabilizing energy reported for the spin-spiral states.

The equilibrium volume is $V = 11.0$ Å^3, the corresponding antiferromagnetic moment is $\mu = 1.35\mu_B$ in a reasonable agreement with the experimental estimate.[40] The generalized-gradient corrections increase the volume by ~ 0.9 Å^3 and lead to a larger volume. Experimental values of the atomic volume are available only for the stable high-temperature phase, $V(\text{exp.}) = 14.6$ Å^3 at $T = 1413$ K. For the antiferromagnetic δ-Mn, we calculate a bulk modulus of $B_0 = 166$ GPa, and a pressure derivative of $B_0' = 6.7$, i.e., values comparable to those of the γ-phase. Moruzzi *et al.*[29] report a bulk modulus of 260 GPa for ferromagnetic δ-Mn (which is the ground state according to their calculations). Asada reports conflicting results in the two publications cited under Ref. 24: a ferromagnetic ground state with a very high bulk modulus of 248 GPa, and an antiferromagnetic (type-1)

ground state with two different values for the bulk modulus: 77 and 150 GPa, respectively. This clearly demonstrates the difficulty of obtaining well-converged results, given the small magnetic energy differences and the strong volume dependence of magnetism.

C. Hexagonal close-packed ϵ-Mn

For ϵ-Mn, the paramagnetic and antiferromagnetic phases are found to be energetically degenerate at equilibrium ($V = 10.5$ Å^3), the axial ratio of the hexagonal-close packed structure is very close to the ideal value of $c/a = 1.633$. A ferromagnetic solution exists only for $V \sim 14$ Å, the paramagnetic to ferromagnetic transition is of first order. The variation of the total energy and of the magnetic moment as a function of volume is more complex as expected for a simple second-order transition—the inflections in both the energy- and the moment-curves at $V \sim 13$ Å^3 are indicative for a sluggish low- to high-spin transition.

It is remarkable that in spite of the same nearest-neighbor environment, magnetism is less stable in ϵ-Mn than in γ-Mn. This shows that exchange interactions beyond nearest neighbors must be considered. In this respect, the structure-property correlation in Mn is similar to that in Fe, where an antiferromagnetic and a nonmagnetic ground state have been predicted for the fcc and hcp phases, respectively. We also find that in the bcc γ-Mn, ferromagnetism persists (although in a low-spin state) up to densities where it is already completely quenched in the other polymorphs. However, in contrast to Fe, the magnetic ground state of the bcc Mn is type-2 antiferromagnetic.

Antiferromagnetic ϵ-Mn has a bulk modulus of $B_0 = 246$ GPa which is comparable to that of the nonmagnetic phases of the other polymorphs—for this structure, the influence of magnetism on the compressibility is rather weak (see also the energy vs volume data in Fig. 4). The pressure derivative of $B_0' = 5.1$ is much lower than that of fcc and bcc Mn and also somewhat lower than that calculated for the α phase—this will turn out to be important for the phase behavior under pressure. Asada *et al.*[24] report values of 242 and 264 GPa for marginally antiferromagnetic hcp Mn in the two sets of calculations.

Altogether the comparison of our GGA results with those obtained in the LSDA shows that the gradient corrections to the exchange-correlation functional largely improve the predictions of the magnetic ground state of the highly symmetric polymorphs of Mn. Because of the enormous computational effort, we have not compared the LSDA and the GGA for the α- and β-phases, but it is evident that here also the gradient corrections are necessary to achieve a reasonable prediction of the atomic volume.

IV. PHASE STABILITY AND PHASE TRANSITIONS

Structural enthalpy differences at zero pressure between the five polymorphs of Mn in their respective magnetic ground states are summarized in Table II: at zero pressure, α-Mn is lower in energy by 63 meV/atom than β-Mn, 67 meV/atom than γ-Mn, 61 meV/atom than ϵ-Mn, and 146 meV/atom than δ-Mn. The stability of the complex α structure is only partly related to magnetic effects: even nonmagnetic α-Mn is still 38 meV/atom lower in energy than β-Mn. This is partly in contradiction to speculations in the current literature on the origin of the stability of the α-phase, but necessary for explaining the stability of paramagnetic α-Mn up to a temperature which is ten times higher than its Néel temperature.

The structural energy differences vary strongly with volume: under compression, all energy differences are strongly reduced, but only for hcp ϵ-Mn the reduction is strong enough such that a pressure-induced phase transition becomes possible. The different elastic behavior of the competing phases is important for understanding that the transition occurs to the hcp and not to the fcc phase, which is comparable in energy around equilibrium. Although fcc γ-Mn is initially much softer than hcp ϵ-Mn, its bulk modulus hardens very rapidly under compression, leading to an increase of the internal energy. On expansion, the energy difference between the α and γ the phases is progressively reduced, whereas the β and ϵ the phases become energetically less favorable. Without the energy lowering associated with the formation of a noncollinear spin structure, γ-Mn would even become favored over α-Mn under sufficiently strong expansion. This is important for understanding the stabilization of the γ phase on alloying with elements inducing a lattice expansion.

The variations in the energy differences are generally quite strongly related to magnetic effects, in particular to the slow onset of magnetism in hcp Mn (see Fig. 4) and in β-Mn (see Fig. 2). Only little change is observed in the energy difference between the α and δ the phases. Figure 5 also illustrates again the contrast, already evident from the calculation of the bulk moduli, between the mechanically soft γ and δ phases and the hard β and ϵ phases, with α-Mn in between. We have already emphasized the relation between the onset of magnetic-moment formation and the elastic properties.

A. Pressure-induced phase transition

Figure 5 suggests that under compression a phase transition from α- to ϵ-Mn will occur. The fact that the hcp phase is favored under compression over the fcc and bcc phases, agrees with the calculations of Zheng-Johansson *et al.*,[25] but the energy differences are so small that it is impossible to determine the transition pressure from a double-tangent construction to the energy vs volume curves. We have used the fitted Birch-Murnaghan and Vinet equations of state (already used for the calculation of the bulk moduli) to calculate the variation of the enthalpy of the α and ϵ the phases as a function of pressure—the critical pressure for the phase transition is than given by the intersection of the enthalpy curves. Our result is displayed in Fig. 6 (both fits lead to identical results, we display only that relating to the Birch-Murnaghan[65] equation of state). As both enthalpy curves have almost the same slope (the difference in the bulk moduli is rapidly reduced under compression, since the pressure derivative of B_0 is larger for the α than for the β phase:

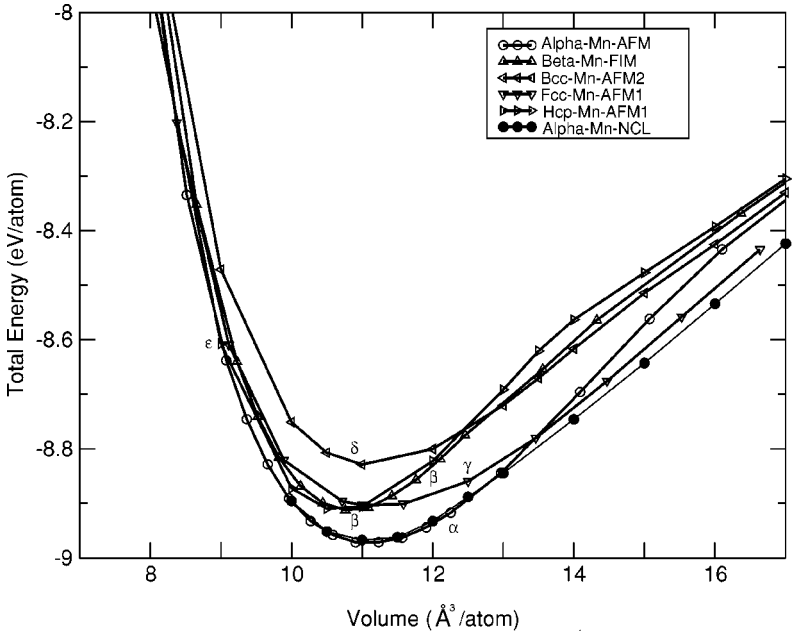

FIG. 5. Total energy of all five polymorphs of Mn as a function of volume. The different symbols represent the calculated energies, for each structure the energy of the magnetic phase stable at the given volume has been plotted—only for α-Mn the energies of both the collinear and the noncollinear antiferromagnetic configurations have been plotted. AFM—antiferromagnetic (type-1 or type-2), FIM—ferrimagnetic, NCL—noncollinear.

$B_0'=5.9$ for α-Mn, $B_0'=5.1$ for ϵ-Mn, the experimental value[21] reported for α-Mn is $B_0'=4.6$), their crossing point is rather ill defined—$p_c \sim 75 \pm 25$ GPa at $T=0$ K seems to be a reasonable estimate. At the transition, the volume discontinuity is very small, about 1%. The small volume change compares well with the experimental estimate of a discontinuity of about 2%. The estimated transition pressure is about a factor 2 lower than the transition pressure of 158–165 GPa at room temperature reported by Fujihisa *et al.*[21] However, in view of the smallness of the energy differences and the complexity of the systems involved, we consider this as a not unreasonable agreement. Increasing the structural energy difference between α- and ϵ-Mn by only 10–15 meV/atom would be sufficient to eliminate the discrepancy between the theory and the experiment. In view of the much larger bulk modulus of ϵ-Mn compared to the α-phase, even the difference in the zero-point vibrational energies could provide a substantial part of the increase in the structural energy difference, cf. also the following paragraph.

In *I*, we have found that the antiferromagnetism of α-Mn disappears under compression at a volume of 9 Å^3 (cf. Fig. 2 in *I*). From our equation of state, we find that this volume corresponds quite exactly to the critical pressure for the structural phase transition. The hcp- Mn, on the other hand, is only marginally magnetic at equilibrium, antiferromagnetism disappears already under slight compression, from our results shown in Figs. 4 and 6, we estimate the antiferromagnetic to nonmagnetic transition in ϵ-Mn to occur al-

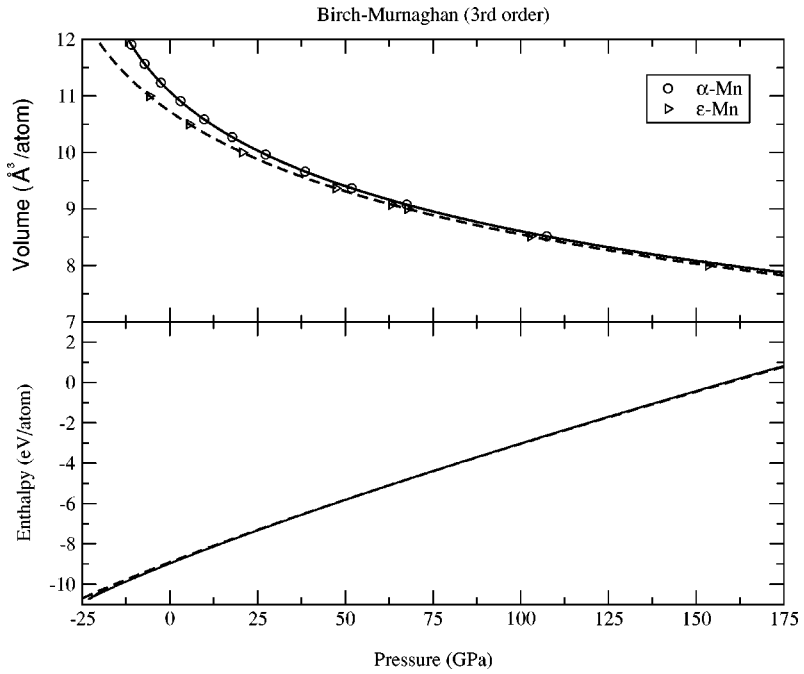

FIG. 6. Equation of state (top panel) and enthalpy of α- and ϵ-Mn as a function of pressure. Circles and triangles represent the pressure-volume relation for the *ab initio* calculations, the continuous solid and broken lines a fit of these data by a third-order Birch-Murnaghan equation or the universal equation of state of Vinet *et al.* (both fits are indistinguishable at the scale of the plot).

ready below 10 GPa. Hence, magnetic effects are very important for the surprising stability of the complex α-Mn structure up to ultrahigh pressures.

B. Temperature-driven phase transitions

Under increasing temperature, Mn undergoes a sequence of structural phase transitions: $\alpha \rightarrow \beta \rightarrow \gamma \rightarrow \delta$. Although temperature effects are not directly considered in this work, we can still make a few comments on temperature-driven phase transitions. The temperature evolution of the equilibrium states is determined by the free energy $F=E-TS$, *i.e.*, from the internal energy we have to subtract the entropy multiplied by the temperature. The entropy consists of a vibrational contribution and a contribution from the fluctuating magnetic moment. Asada and Terakura[24] have made an attempt to investigate the temperature-dependent phase transitions between the γ, δ, and ϵ phases on the basis of *ab initio* total-energy calculations coupled to a quasiharmonic Debye-Grüneisen model for the vibrational entropy. Following Moruzzi, Janak, and Schwarz,[69] the Debye-temperature Θ was estimated from the bulk modulus using a semiempirical relation, the volume-dependence of Θ was determined by using a relation between the pressure derivative of the bulk modulus and the Grüneisen parameter. It must be emphasized that this is a rather crude model, since not only the bulk modulus but also the shear constants determine the Debye temperature. However, it may serve as a first approximation for a qualitative estimate of the relative importance of vibrational and magnetic contributions to the entropy. Within this model, the low values of the bulk modulus of γ- and δ-Mn lead to a much lower Debye temperature and hence to a faster increase of the vibrational entropy for these two phases than for ϵ-Mn, changing the energetic order between the fcc and the hcp phases already at modest temperatures.[24]

Due to the large difference in the bulk moduli, even zero-point vibrations could influence the pressure-induced phase transition between the α and ϵ the phases. Using the semiempirical relation of Moruzzi, Janak, and Schwarz[69] and the bulk moduli listed in Table II, we calculate Debye temperatures of $\Theta(\alpha)=393$ K and $\Theta(\epsilon)=468$ K, leading to a difference of 5.3 meV/atom in the zero-point energies, which adds to the structural energy difference and leads to an increased critical pressure of $p_c \sim 100 \pm 25$ GPa at $T=0$ K. Using the same values of the Debye temperatures to calculate the contribution of the vibrational entropy to the free energies at $T=300$ K, we obtain a further contribution to the structural energy difference of about 7 meV/atom favoring the α phase and leading to a further increase of the transition pressure. However, above the Néel temperature, we have to use the larger bulk modulus (see also *I*) and Debye temperature of nonmagnetic α-Mn, leading to a much smaller difference in the vibrational entropies.

However, it also becomes clear that vibrational effects alone are not sufficient to reverse the energetic ordering between the fcc and the bcc Mn. In this respect, the magnetic contributions to the entropy will be important—the smallness of the magnetic energy differences in the bcc δ-Mn (cf. Fig. 4) suggests a larger magnetic contribution to the entropy for δ- than for γ-Mn. Magnetic effects will also influence the $\alpha \rightarrow \beta$ transition. Below the Néel temperature antiferromagnetic α-Mn is much softer than β-Mn, hence vibrational effects will even add to the structural energy difference. For a paramagnetic α-Mn, our calculations predict a much harder bulk modulus of nearly 300 GPa—at least as long as magnetic fluctuations are neglected. However, the difference in the compressibilities of nonmagnetic α- and β-Mn ($\Delta B_0 \sim 20-30$ GPa) appears to be too small to attribute the phase change to vibrational effects alone. The strong paramagnetic fluctuations in β-Mn arising from geometric frustrations have already been mentioned. Magnetic fluctuations exist also in α-Mn. Neutron-scattering experiments[70] of very dilute alloys of Sn in α-Mn have demonstrated a very different temperature dependence of the magnetic moments of the crystallographically inequivalent atoms: the Mn I moments even increase slightly with temperature and their ordering disappears at the Néel temperature after going through a maximum, the Mn II moments decrease rapidly, becoming disordered already below the Néel temperature. The moments on the Mn IV sites could even change sign with increasing temperature. All this is indicative of large magnetic fluctuations already in the antiferromagnetic state and it must be expected that magnetic fluctuations exist also in the paramagnetic state. Hence, the magnetic entropy will favor β-Mn, but only to a sufficiently modest degree to explain the stability of α-Mn up to a temperature of $T_{\alpha \rightarrow \beta}=1000$ K which is substantially higher than the temperature corresponding to the structural energy difference [$\Delta E(\alpha \rightarrow \beta) \equiv T \sim 730$ K].

V. SUMMARY AND CONCLUSIONS

This paper concludes our comprehensive investigation of the structural, magnetic, and electronic properties of Mn, which may with a good reason be considered as the complex metallic element. We have demonstrated that the complex crystalline and magnetic structures of the α and β phases result from conflicting physical effects associated with the half-filled $3d$ band. According to the Friedel model of transition-metal bonding, at half filling only bonding and no antibonding states are occupied, maximizing the cohesive energy and minimizing the interatomic distances. However, the Friedel model ignores spin polarization, whereas according to Hund's rule for a half-filled band, the parallel alignment of all spins leads to a maximum of the magnetic spin moment. If spin polarization is complete, both bonding and antibonding linear combinations of spin-up *d* states are completely occupied, and all spin-down states are empty. The magnetically induced occupation of antibonding states tends to expand the crystal. In reality, because of the rather large width of the *d* band and because of *sd* hybridization, Mn is quite far from the limit set by Hund's rule. In α- and β-Mn, nature tries to cope with these conflicting tendencies by adopting topologically close-packed polytetrahedral structures in which crystallographically inequivalent lattice sites are coordinated either by distorted tetrahedra (the sites admitting only small atoms) or larger Frank-Kasper CN14 and Friauf CN16 polyhedra that admit larger atoms on their cen-

tral sites and also give rise to a distorted polytetrahedral close packing and therefore good space filling. The locally increased packing density at the center of the icosahedra leads to a broadening of the *d* band and reduces (or even quenches) the local magnetic moment. It is significant that the *A*12 and *A*13 structures of α- and β-Mn are assumed quite frequently by intermetallic compounds formed by large and small atoms (*A*12: χ-phase Ti_5Re_{24}, γ-$Mg_{17}Al_{12}$; *A*13: Fe_2Re_3).

As a consequence of the polytetrahedral atomic arrangement with only triangular facets on the surface of the coordination polyhedra, the antiferromagnetic exchange interactions between the Mn-atoms are at least locally frustrated. In α-Mn, the frustration is strongest in the Mn IV triangles on the surface of the CN16 polyhedra surrounding the Mn I atoms with the highest magnetic moments. The Mn IV–Mn IV distances are also the shortest interatomic distances in this structure. At high densities, the Mn IV moment is completely quenched. We have found that this is sufficient to release the magnetic frustration and to stabilize a collinear antiferromagnetic structure. At lower densities, the Mn IV atoms become magnetic (the local nonmagnetic to antiferromagnetic transition is of second order) and the Mn IV moments adopt on each triangle a local configuration similar to that of nearest-neighbor spins in the Néel phase of a frustrated triangular antiferromagnet. The coupling to the other Mn sites drives the noncollinearity of the antiferromagnetic α-Mn structure, which increases in proportion to the magnitude of the Mn IV moments. The alternative to the canting of the magnetic moments would be a large structural distortion—which is, however, energetically not competitive.

The situation is less clear in β-Mn: the geometric difference between the inequivalent Mn sites is now much smaller. An analysis based on the assumption that only the Mn II atoms are magnetic leads to the conclusion that due to the topology of the Mn II sublattice, β-Mn is geometrically frustrated. Our calculations do not support the claim that the Mn I atoms play no role in determining the magnetic properties. As expected from the tighter binding around the Mn I atoms, the magnetic moments on these sites remain smaller than the Mn II moments even on expansion, but the existence of an at least metastable ferrimagnetic state demonstrates that there is a strong antiferromagnetic Mn II-Mn I coupling. At equilibrium, we find the nonmagnetic and weakly ferrimagnetic phases of β-Mn to be energetically degenerate—this is consistent with the experimentally observed spin-liquid behavior and therefore a very flat magnetic potential-energy surface. Of course, this potential-energy surface contains also many degenerate local minima corresponding to noncollinear configurations, but in view of the expected flatness of these minima it is not surprising that the noncollinear calculations fail to converge. Altogether, the Mn-based Laves phases should be considered as a better reference for discussing geometric frustration in β-Mn than the ''three-dimensional Kagomé'' sublattice of the Mn II atoms alone. The difference in the magnetic behavior is also reflected in the elastic properties, with ''soft'' α-Mn in contrast to ''hard'' β-Mn.

Magnetic frustration also plays an important role in the highly symmetric Mn polymorphs. Both in fcc γ-Mn and in bcc δ-Mn, our calculations show that the paramagnetic and different antiferromagnetic phases are extremely close in energy at equilibrium. The gain in magnetic energy upon even a very slight expansion significantly influences the equation of state and contributes to the exceptional elastic softness of both γ-Mn and δ-Mn. The hcp ϵ-Mn, on the other hand, is only marginally magnetic at equilibrium and this is reflected in a much harder modulus of compression.

Under compression, our calculations predict a transition from the α to the ϵ phase, at a critical pressure which is at least in reasonable agreement with experiment if the difference in the zero-point energies is added to the structural energy difference. The persistence of the antiferromagnetism in α-Mn up to a very high pressure is a very surprising result, but essential for stabilizing the α phase. The hcp structure is favored under compression over the other two common metallic structures, agrees with the regular structural trend in the $4d$ and $5d$ series. Our comments on temperature-driven phase transitions are admittedly speculative, but the essential role of magnetic fluctuation is certainly real.

The ability to explain the structural trends across the periodic table is certainly one of the important successes of density-functional theory,[71–73] the present study fills one of remaining white spots—Mn. Although our investigations predict the correct energetic order between the different phases, explain the origin of noncollinearity in α-Mn and the nature of the pressure-induced phase transition, agreement with experiment is not perfect: in all phases we find the equilibrium volume to be underestimated. Generalized-gradient corrections to the exchange-correlation functional represent an important improvement, but similarly as for the neighboring antiferromagnetic element in the periodic table, Cr, they are not sufficient to completely close the gap between theory and experiment.

ACKNOWLEDGMENTS

This work has been supported by the European TMR Network ''Electronic Structure Calculations for Industry and Basic Sciences'' (Contract No. ERB FMRX CT 98-0178) and by the Center for Computational Materials Science. Useful discussions with Daniel Spišák and Georg Kresse are gratefully acknowledged.

[1] J. Donohue, *The Structures of the Elements* (Wiley, New York, 1974).

[2] R. R. Tebbe and D. J. Gaik, *Magnetic Materials* (Interscience, London, 1969).

[3] A.J. Bradley and J. Thewlis, Proc. R. Soc. London, Ser. A **115**, 465 (1927).

[4] T. Yamada, N. Kunitomi, Y. Nakai, D.E. Cox, and G. Shirane, J. Phys. Soc. Jpn. **28**, 615 (1970).

[5] T. Yamada, J. Phys. Soc. Jpn. **28**, 596 (1970).

[6] A.C. Lawson, A.C. Larson, M.C. Aronson, S. Johnson, Z. Fisk,

P.C. Canfield, J.D. Thomson, and R.B. van Dreele, J. Appl. Phys. **76**, 7049 (1994).
[7] G.D. Preston, Philos. Mag. **5**, 1207 (1928).
[8] M. O'Keefe and S. Anderson, Acta Crystallogr., Sect. A: Cryst. Phys., Diffr., Theor. Gen. Crystallogr. **A33**, 914 (1977).
[9] J.S. Kasper and B.W. Roberts, Phys. Rev. **101**, 537 (1956).
[10] Y. Masuda, K. Asayama, S. Kobayashi, and J. Itoh, J. Phys. Soc. Jpn. **19**, 460 (1964).
[11] H. Nakamura, K. Yoshimoto, M. Shiga, M. Nishi, and K. Kakurai, J. Phys.: Condens. Matter **9**, 4701 (1997).
[12] T. Shinkoda, K. Kumagai, and K. Asayama, J. Phys. Soc. Jpn. **46**, 1754 (1979).
[13] M. Katayama, S. Akimoto and K. Asayama, J. Phys. Soc. Jpn. **42**, 97 (1977).
[14] Y. Kohori, Y. Iwamoto, Y. Muro, and T. Kohara, Physica B **237–238**, 455 (1997).
[15] T. Oguchi and A.J. Freeman, J. Magn. Magn. Mater. **20**, 107 (1980).
[16] T. Jo and K. Hirai, J. Phys. Soc. Jpn. **55**, 2017 (1986).
[17] H. Uchishiba, J. Phys. Soc. Jpn. **31**, 436 (1971).
[18] M. Wuttig, Y. Gauthier, and S. Blügel, Phys. Rev. Lett. **70**, 3619 (1993).
[19] O. Rader, W. Gudat, C. Carbone, E. Vescovo, S. Blügel, R. Kläsges, N. Eberhardt, M. Wuttig, J. Redinger, and F.J. Himpsel, Phys. Rev. B **55**, 5404 (1997).
[20] B. Heinrich, A.S. Arrott, J.F. Cochran, C. Liu, and K. Myrtle, J. Vac. Sci. Technol. A **4**, 1376 (1986).
[21] H. Fujihisa and K. Takemura, Phys. Rev. B **52**, 13 257 (1995).
[22] H. Skriver, Phys. Rev. B **31**, 1909 (1985).
[23] A.T. Paxton, M. Methfessel, and H.M. Polatoglu, Phys. Rev. B **41**, 8127 (1990).
[24] T. Asada and K. Terakura, Phys. Rev. B **47**, 15 992 (1993); T. Asada, in *Interatomic Potential and Structural Stability*, edited by K. Terakura and H. Akai (Springer, Berlin, 1993), p. 201 ff.
[25] J.X. Zheng-Johansson, O. Eriksson, B. Johansson, L. Fast, and R. Ahuja, Phys. Rev. B **57**, 10 989 (1995).
[26] R. Hafner, D. Spišák, R. Lorenz, and J. Hafner, J. Phys.: Condens. Matter **13**, L239 (2001).
[27] See, e.g., E.G. Moroni, G. Kresse, J. Furthmüller, and J. Hafner, Phys. Rev. B **56**, 15 629 (1997), and further references cited therein.
[28] J. Kübler, J. Magn. Magn. Mater. **20**, 107 (1980).
[29] V.L. Moruzzi, P.M. Marcus, and P.C. Pattnaik, Phys. Rev. B **37**, 8003 (1988).
[30] V.L. Moruzzi and P.M. Marcus, Phys. Rev. B **38**, 1613 (1988).
[31] S. Fujii, S. Ishida, and S. Asano, J. Phys. Soc. Jpn. **60**, 1193 (1991).
[32] V.L. Moruzzi and P.M. Marcus, Solid State Commun. **71**, 203 (1989).
[33] V.L. Moruzzi, P.M. Marcus, and J. Kübler, Phys. Rev. B **39**, 6957 (1989).
[34] G. Fuster, N.E. Brener, J. Callaway, J.L. Fry, Y.Z. Zhao, and D.A. Papaconstantopoulos, Phys. Rev. B **38**, 423 (1988).
[35] P. Blaha, K. Schwarz, and P. Dederichs, Phys. Rev. B **38**, 9368 (1988).
[36] M. Podgorny and J. Goniakowski, Phys. Rev. B **42**, 6683 (1990).
[37] V.L. Sliwko, P. Blaha, P. Mohn, and K. Schwarz, Int. J. Quantum Chem. B **7**, 614 (1993).
[38] P. Mohn, K. Schwarz, M. Uhl, and J. Kübler, Solid State Commun. **102**, 729 (1997).
[39] M. Eder, J. Hafner, and E.G. Moroni, Phys. Rev. B **61**, 11 492 (2000).
[40] J.B. Goodenough, Phys. Rev. **120**, 67 (1960).
[41] Y. Endoh and Y. Ishikawa, J. Phys. Soc. Jpn. **30**, 1641 (1971).
[42] V. Sliwko, P. Mohn, and K. Schwarz, J. Phys.: Condens. Matter **6**, 6557 (1994).
[43] V.P. Antropov, M. van Schilfgaarde, and B.N. Harmon, J. Magn. Magn. Mater. **140–144**, 1355 (1995).
[44] T. Asada, J. Magn. Magn. Mater. **140–144**, 47 (1995).
[45] F. Süss and V. Krey, J. Magn. Magn. Mater. **125**, 351 (1993).
[46] D. Hobbs and J. Hafner, J. Phys.: Condens. Matter **13**, L681 (2001).
[47] D. Hobbs, J. Hafner, and D. Spišák, preceding paper, Phys. Rev. B **68**, 014407 (2003).
[48] B. Canals and C. Lacroix, Phys. Rev. B **61**, 11 251 (2000).
[49] P.W. Anderson, B. Halperin, and C.M. Varma, Philos. Mag. **25**, 1 (1972).
[50] J.N. Reimers, Phys. Rev. B **45**, 7287 (1992).
[51] B. Canals and C. Lacroix, Phys. Rev. Lett. **80**, 2933 (1998).
[52] R. Moessner and J.T. Chalker, Phys. Rev. Lett. **80**, 2929 (1998).
[53] C.B. Shoemaker, D.P. Shoemaker, T.E. Hopkins, and S. Yindepit, Acta Crystallogr., Sect. B: Struct. Crystallogr. Cryst. Chem. **34**, 3573 (1978).
[54] P.E. Blöchl, Phys. Rev. B **50**, 17 953 (1994).
[55] G. Kresse and D. Joubert, Phys. Rev. B **59**, 1758 (1999).
[56] D. Hobbs, G. Kresse, and J. Hafner, Phys. Rev. B **62**, 11556 (2000).
[57] J.P. Perdew and A. Zunger, Phys. Rev. B **23**, 5048 (1981).
[58] U. von Barth and L. Hedin, J. Phys. C **5**, 1629 (1972).
[59] J.P. Perdew, J.A. Chevary, S.H. Vosko, K.A. Jackson, M.R. Pedersen, D.J. Singh, and C. Fiolhais, Phys. Rev. B **46**, 6671 (1992).
[60] J. Villain, Z. Phys. B **33**, 31 (1979).
[61] M. Shiga, J. Magn. Magn. Mater. **129**, 17 (1994).
[62] R. Ballo, C. Lacroix, and D. Nurez-Regueiro, Phys. Rev. Lett. **66**, 1910 (1991).
[63] Y. Kohori, Y. Noguchi, and T. Kohara, J. Phys. Soc. Jpn. **62**, 447 (1993).
[64] C. Herring, in *Magnetism IV*, edited by G. T. Rado and H. Suhl (Academic Press, New York, 1966), pp. 81, 298.
[65] F.D. Murnaghan, Proc. Natl. Acad. Sci. U.S.A. **3**, 244 (1944); F. Birch, J. Geophys. Res. **57**, 227 (1952).
[66] P. Vinet, J.R. Smith, J. Ferrante, and J.H. Rose, Phys. Rev. B **35**, 1945 (1987).
[67] N.A. Cade and W. Young, Met. Phys. **10**, 2035 (1980).
[68] R. W. G. Wyckoff, *Crystal Structure* (Wiley, New York, 1963); and in *Magnetic Properties of Metals*, edited by H. P. J. Wijn, Landolt-Börnstein, New Series, Group III, Vol. 19, Pt. a (Springer, Berlin, 1971), p. 17.
[69] V.L. Moruzzi, J.F. Janak, and K. Schwarz, Phys. Rev. B **37**, 790 (1988).

[70] Y. Nakai and Y. Tsunoda, J. Phys. Soc. Jpn. **64**, 1748 (1995).
[71] J. Hafner and V. Heine, J. Phys. F: Met. Phys. **13**, 2479 (1983).
[72] J. Hafner, in *The Structures of Binary Compounds*, edited by F. R. de Boer and D. G. Pettifor (North Holland, Amsterdam, 1989), p. 147 ff; J. A. Majewski and P. Vogl, *ibid*, p. 287.
[73] D.G. Pettifor, J. Phys. C **3**, 367 (1970); J. Phys. F: Met. Phys. **7**, 613 (1977).